Published in final edited form as:
Neuroimage. 2018 March ; 168: 490–498. doi:10.1016/j.neuroimage.2016.12.070.

The clinical relevance of distortion correction in presurgical fMRI at 7 T

Pedro Lima Cardoso[a], **Barbara Dymerska**[a], **Beáta Bachratá**[a], **Florian Ph.S. Fischmeister**[a,b], **Nina Mahr**[a,b], **Eva Matt**[a,b], **Siegfried Trattnig**[a], **Roland Beisteiner**[a,b], and **Simon Daniel Robinson**[a,*]

[a]High Field Magnetic Resonance Centre, Department of Biomedical Imaging and Image-guided Therapy, Medical University of Vienna, Lazarettgasse 14, A-1090 Vienna, Austria

[b]Study Group Clinical fMRI, Department of Neurology, Medical University of Vienna, Währinger Gürtel 18-20, A-1090 Vienna, Austria

Abstract

Presurgical planning with fMRI benefits from increased reliability and the possibility to reduce measurement time introduced by using ultra-high field. Echo-planar imaging suffers, however, from geometric distortions which scale with field strength and potentially give rise to clinically significant displacement of functional activation.

We evaluate the effectiveness of a dynamic distortion correction (DDC) method based on unmodified single-echo EPI in the context of simulated presurgical planning fMRI at 7 T and compare it with static distortion correction (SDC). The extent of distortion in EPI and activation shifts are investigated in a group of eleven patients with a range of neuropathologies who performed a motor task. The consequences of neglecting to correct images for susceptibility-induced distortions are assessed in a clinical context.

It was possible to generate time series of EPI-based field maps which were free of artifacts in the eloquent brain areas relevant to presurgical fMRI, despite the presence of signal dropouts caused by pathologies and post-operative sites. Distortions of up to 5.1 mm were observed in the primary motor cortex in raw EPI. These were accurately corrected with DDC and slightly less accurately with SDC. The dynamic nature of distortions in UHF clinical fMRI was demonstrated via investigation of temporal variation in voxel shift maps, confirming the potential inadequacy of SDC based on a single reference field map, particularly in the vicinity of pathologies or in the presence of motion. In two patients, the distortion correction was potentially clinically significant in that it might have affected the localization or interpretation of activation and could thereby have influenced the treatment plan.

Distortion correction is shown to be effective and clinically relevant in presurgical planning at 7 T.

*Correspondence to: High Field Magnetic Resonance Centre, Medical University of Vienna, Lazarettgasse 14/BT32, A-1090 Vienna, Austria. simon.robinson@meduniwien.ac.at (S.D. Robinson).

Europe PMC Funders Author Manuscripts

Keywords

Dynamic distortion correction; fMRI; Presurgical planning; Ultra-high field; Patients; Motor

1 Introduction

Functional brain networks can be rapidly and non-invasively localized using functional MRI (fMRI), making it an attractive modality in presurgical mapping in patients with brain tumors and epilepsy. The aim is to allow neurosurgeons to identify relevant anatomical landmarks (e.g. the central sulcus for the motor function), which demarcate brain regions that should be preserved in the excision of pathological tissue or epileptogenic foci in order to avoid post-surgical deficits. Functional localization is of special interest in diseased brains, in which normal cortical anatomy may be distorted by the pathology due to mass effects, hindering the easy identification of these landmarks (Lehericy et al., 2000). The most common tasks recruit motor, somatosensory, language, and memory function, and good correlation has been demonstrated between fMRI results and ‘gold standard’ methods (Adcock et al., 2003; Binder et al., 1996; Kashida et al., 2016; Stevens et al., 2016).

Presurgical planning with fMRI benefits from increased reliability and the possibility to reduce measurement time introduced by using ultra-high field (UHF), due to the higher signal-to-noise ratio (SNR) and increased blood-oxygen-level dependent (BOLD) contrast (Beisteiner et al., 2011; Triantafyllou et al., 2005; van der Zwaag et al., 2009). Echo-planar imaging (EPI) suffers, however, from geometric distortion mostly in the phase-encoding direction (Jezzard and Balaban, 1995) in the presence of susceptibility-related field inhomogeneities which lead to mislocalization of activation (Cusack et al., 2003). Distortion scales linearly with field strength, making it important that an accurate correction be used at UHF. This is of particular relevance in the context of presurgical planning, in which potential shifts in activation caused by geometric distortion may lead to misidentification of essential functional landmarks and impact the surgical approach (Dymerska et al., 2014; Robinson et al., 2010). Therefore, accurate determination of these landmarks is of utmost importance prior to surgery. During the surgical procedure itself, cortical tissue displacements greater than 10 mm have been reported due to brain surface deformation following craniotomy. However, to mitigate this problem, relevant anatomical landmarks or surfaces determined a *priori* may be labelled correctly after bone flap removal to enable tracking of deformation during the operation (Hill et al., 1998; Roberts et al., 1998).

Distortions in fMRI are typically corrected with a “static” approach, in which a map of local deviations from the static magnetic field, B_0, is acquired prior to or subsequent to fMRI runs (Jezzard and Balaban, 1995; Robinson and Jovicich, 2011). This approach fails, however, to capture changes in B_0 which occur during the fMRI acquisition due to motion (Jezzard and Clare, 1999), respiration (Zahneisen et al., 2014; Zeller et al., 2014), or heating of the gradient system (Foerster et al., 2005).

One dynamic approach to correcting susceptibility-related distortions is to model susceptibility-by-movement effects (Andersson et al., 2001), although this neglects non-motion sources such as respiration. Alternatively, a time-series of B_0 field maps can be

extracted from the phase of the fMRI data if a multi-echo EPI sequence is used (Hutton et al., 2002; Poser and Norris, 2009; Visser et al., 2012; Weiskopf et al., 2005). This, however, constrains the achievable spatial resolution, particularly with short T_2* at UHF. Field maps can also be derived from adjacent time points in single-echo EPI if the TE is 'jittered' between two values (Dymerska et al., 2016b). Alternatively, Hahn et al. (2009) and Ooi et al. (2013) proposed single-echo EPI-based dynamic approaches, in which field changes between a reference or mean volume and the rest of the EPI time series are calculated. Up to 3 T, these methods allow phase unwrapping to be avoided since phase difference values are typically within 2π. This is not the case at 7 T, however (Dymerska et al., 2016a). The Hahn et al. and Ooi et al. approaches also have the disadvantage that a second unwarping step is required to remove distortions present in the reference time point image, which requires a static field map. Marques and Bowtell (2005) and Lamberton et al. (2007) outlined how field maps can be derived from an unmodified, single-echo EPI time series if the non-B_0-related contributions to the total EPI phase (the receiver phase offsets (Robinson et al., 2011)) are known. This approach has been further developed to yield robust results for array coils at UHF and large motion (Dymerska et al., 2016a) but has not yet been applied in a clinical context. Brain tumors and post-operative sites are highly heterogeneous in composition, and can be expected to generate larger field offsets and higher gradients in the field than are observed in the general population, leading to large distortions and signal dropout. These can be anticipated to prove challenging to remove phase wraps from, due to signal voids (Robinson et al., 2016), and distortion-correct, due to the need for substantial interpolation and correct treatment of signal which is "piled up" or swapped across a boundary (Robinson and Jovicich, 2011).

Dynamic distortion correction (DDC) is applied in this study in a cohort of patients with diverse brain pathologies who performed a motor task at 7 T and compared with a static conventional approach based on gradient echo field mapping. The extent of distortions in EPI at UHF, the effectiveness of distortion correction in the presence of pathologies, and the potential clinical implications of carrying out presurgical planning on the basis of 7 T fMRI results without correcting the mislocalization of activation are assessed.

2 Materials and Methods

This study was designed to assess the effectiveness of a dynamic correction of susceptibility-related distortions in simulated presurgical fMRI in a clinical population performing a motor task and compare it with a conventional static distortion correction (SDC) approach. The potential impact of the correction on a presurgical treatment plan was evaluated. The geometry of EPI images before and after distortion correction were compared with a distortion-free gradient echo (GE) reference scan within the primary target region – the motoric cortex. Mislocalization of activation due to distortion was identified by comparing functional maps generated with uncorrected and distortion-corrected data overlaid on a GE reference image.

Europe PMC Funders Author Manuscripts

2.1 Participants

Candidate patients were contacted by physicians from the Departments of Internal Medicine (Division of Oncology) and Neurosurgery of the Vienna General Hospital and from the Neurology Department of the Wilhelminenspital, Vienna, and the Neurosurgery Department of the Rudolfstiftung, Vienna. Written informed consent was provided by all participants, and the study was approved by the Ethics Committee of the Medical University of Vienna.

All 12 patients (mean age 46 ± 12 years old, 7 females) were in a good general state of health at the time of measurement and were able to perform the task. One female patient aged 62 with an oligoastrocytoma in the right parieto-frontal region was excluded from this study due to excessive motion. Patient demographics and clinical details are given in Table 1.

2.2 Task

Patients were asked to perform up to 10 runs (depending on tolerance) of a hand paradigm in a block design, except for one patient (P1), who performed an elbow task and P6, who only completed 9 runs of the hand paradigm. Each run consisted of 4 rest and 3 movement phases of 20 s each, presented in a ABABABA design (A: rest phase; B: task phase). The hand task comprised alternated opening and closing of the hand; the elbow task flexion and extension of the elbow. Visual cues specifying when to start and stop movement and the desired repetition frequency were presented using the software Presentation (Neurobehavorial Systems, Albany, USA), which was triggered by the MRI scanner. In the task condition, the cues consisted of the words “LINKS” or “RECHTS” (the German for “LEFT” and “RIGHT”, respectively) in yellow text blinking at a frequency of 0.5 Hz on a black background. The rest condition was a white crosshair on a black background.

2.3 Data acquisition

Imaging was performed at 7 T with a Siemens MAGNETOM scanner (Siemens Healthcare, Erlangen, Germany) and a 32-channel head coil (Nova Medical, Wilmington, USA). Individually cast plaster helmets were used to minimize head movement (Edward et al., 2000).

Functional MRI data were acquired with a 2D single-shot gradient echo (GE) EPI sequence, with 40 slices of 3 mm thickness and 10% gap, acquired parallel to the AC-PC plane in ascending direction, with a matrix size of 128×128, FOV = 220×220 mm (nominal 1.7×1.7 mm inplane resolution), TE/TR = 22/2500 ms, flip angle (FA) of 75°, receiver bandwidth (RBW) of 1447 Hz/pixel, in-plane acceleration (GRAPPA) of 2, and partial Fourier (PF) encoding of 6/8 (omission of the first 25% of phase-encoding steps). Phase blips were positive in the posterior-anterior direction to avoid signal pile-up around the orbitofrontal cortex (De Panfilis and Schwarzbauer, 2005). Two dummy excitations were used before the acquisition of 57 volumes per run and the first volume was discarded to achieve quasi-equilibrium in longitudinal magnetization.

Multi-echo GE images were acquired twice, once before (GE1) and once after (GE2) the functional runs for field mapping, with geometry and orientation matching that of the

functional runs. The remaining sequence parameters were: TE = [5.0, 10.0, 16.0] ms, TR = 801 ms, FA = 46°, RBW = 230 Hz/pixel, GRAPPA 2, and PF = 6/8.

2.4 Data analysis

The main analysis steps in the processing of uncorrected (noDC), SDC, and DDC EPI time series are schematically illustrated in Fig. 1.

The analysis was implemented in MATLAB (MathWorks, Natick, Massachusetts, USA), unless otherwise specified, and – other than the aspect of distortion – was carried out in the native space of the EPI (i.e. data were not coregistered to a template or structural scan).

For each patient, the time point ("best_TP") was identified from all the EPI time series for which there was least motion with reference to both field maps. The remaining TPs were co-registered to this image. This "best_TP" was determined by realigning all the individual TPs from all the runs to both GE images (GE1 and GE2) using a rigid body (6 degrees of freedom) registration in SPM12 (http://www.fil.ion.ucl.ac.uk/spm/software/spm12/), and selecting the TP with the smallest cumulative rotation (i.e. $\min(|roll| + |pitch| + |yaw|)$) with respect to both GE images. This type of motion has been shown to be the most relevant in introducing susceptibility-induced distortion by movement (Andersson et al., 2001). Rigid body registration was used to avoid mixing distortion correction with image shearing and stretching introduced by affine transformation. As such, susceptibility-related distortions caused by inhomogeneity in B_0 were left visible in registered fMRI runs and their extent at UHF could be assessed in a clinical context. The GE image with the smallest displacement with respect to the "best_TP" is called "GE reference" in subsequent descriptions. This GE scan was used to calculate a field map for SDC and as a reference image which is distortion-free in the phase encoding direction.

In the noDC scheme (Fig. 1, blue), no distortion correction was applied, but each TP was realigned to the "best_TP" using rigid body registration. In the SDC scheme (Fig. 1, green), distortion correction was applied to individual TPs of the fMRI runs using a GE-based static field map (Jezzard and Balaban, 1995; Robinson and Jovicich, 2011). In the DDC scheme (Fig. 1, red), a series of EPI-based field maps (one per TP) were used to separately distortion correct each TP in the fMRI runs (Dymerska et al., 2016a). This was followed by rigid body registration of the distortion-corrected TPs to the "best_TP". No normalization or spatial smoothing was used and single subject GLM analysis was performed, as described in Section 2.5. Details of how the SDC and DDC were performed can be found in Sections 2.4.1 and 2.4.2, respectively.

2.4.1 Static distortion correction (SDC)—The most commonly used method to unwarp EPI into an undistorted space is the "field map" approach described by Jezzard and Balaban (1995). The field distribution (field map) is derived from a GE pre-scan acquired at different echo times in addition to the fMRI runs. In our study, multi-channel GE images from the first two echoes were combined using the Hermitian inner product (Scharnhorst, 2001) and the combined phase was unwrapped within a brain mask with FSL's PRELUDE (Jenkinson, 2003) in 2D. The field map for each patient was obtained by dividing the unwrapped phase by $2\pi \cdot \Delta TE$, smoothed using the MATLAB function "smoothn" (Garcia,

Europe PMC Funders Author Manuscripts

2010) (smoothing parameter = 0.5) and converted into a voxel shift map (VSM). VSMs specify by how many voxels each voxel in the functional data has been distorted in the phase encoding direction. VSMs were obtained by dividing the field map values by the product of the receiver bandwidth in the phase-encoding direction and the parallel imaging acceleration factor used in the EPI time series. The gradient in the VSM in the phase encoding direction was thresholded to a maximum value of 0.9 (values above this were set to 0.9) so that no voxel “jumped over” an adjacent voxel in the unwarping process (Robinson and Jovicich, 2011). Finally, the thresholded VSM together with linear interpolation in the phase encoding direction (with the MATLAB function "interp1") were used to unwarp the magnitude EPI time series.

2.4.2 Dynamic distortion correction (DDC)—Dynamic distortion correction using a time series of field maps derived from the EPI data themselves comprises a series of steps from the derivation of receiver phase offsets from the GE reference scan to the calculation of VSMs. A detailed description of the DDC method can be found in Dymerska et al. (2016a). Briefly, the receiver phase offsets derived from the first two echoes of the GE reference volume (Robinson et al., 2011) were subtracted from each single channel EPI phase image. The resulting phase images were combined using the angle of the complex sum over channels, and unwrapped within a brain mask with FSL's PRELUDE (Jenkinson, 2003) in 2D. A triplanar unwrapping approach (Robinson et al., 2014) was applied in regions with tissue discontinuities (i.e. in the most ventral slices or in regions of pathology with large signal dropout). These unwrapped phase images were smoothed and extrapolated outside of the brain with a discretized spline smoother (MATLAB function “smoothn”, smoothing parameter of 2) and made congruent to the unmasked wrapped combined phase image. A time series of field maps was obtained and applied to the EPI time series as described for the SDC in Section 2.4.1.

2.5 GLM analysis

NoDC, SDC, and DDC data were analyzed with the GLM, using SPM12. High-pass filtering, with a default cut-off frequency of 1/128 Hz, was applied to the data after realignment and before GLM analysis. A canonical HRF was used, with no model derivatives or motion correction regressors.

The third echo of the GE reference (i.e. that with the TE, and hence contrast, closest to that of the EPI) was rigid body realigned to the “best_TP” to yield a reference image which was free of distortion in the phase-encoding direction. Functional activation maps computed for each scheme were overlaid on this reference image.

2.6 Effect of distortion correction on the geometry of the EPI and shifts in activation

The extent of distortion in noDC EPI and the effectiveness of SDC and DDC were assessed for each patient by pairwise comparisons between the distortion-free GE reference image and noDC, SDC, and DDC EPI. Also, the average across the time series of VSMs and the standard deviation of the time series of VSMs were computed in the DDC case, and VSMs generated for SDC inspected. The slice containing the most statistically significant activation in the motor cortex (highest t-value) was selected for assessment. To aid the

visualization of geometric shifts in the hand motor cortex of the ipsilesional side, lines delimiting this anatomical region were drawn using the central sulcus as a reference. In addition, regions of interest (ROIs) encompassing the central sulcus in the selected slice were drawn. SDC and average DDC VSMs were used to investigate the extent of shifts, and the standard deviation of the DDC VSMs their temporal stability across the fMRI time series in these ROIs.

Shifts in activation peaks between noDC, SDC, and DDC were evaluated for each patient. Functional maps were thresholded so that only a few (~2–10) voxels with the highest t-values were visible. These and unthresholded maps were overlaid on GE distortion-free images. All individual noDC, SDC, and DDC functional maps were visually inspected at various thresholds and across slices by a neurologist with extensive clinical fMRI expertise (RB), and the potential clinical relevance in a presurgical planning context of the activation displacement was assessed.

3 Results

3.1 Effect of the distortion correction on EPI geometry

The presence of large complex pathologies, and signal variations or dropouts close to post-operative sites in the pathological brains investigated represents a challenge in the calculation of artifact-free field maps, particularly in the phase unwrapping process. Despite this, the DDC method was able to generate field maps which were, on visual inspection, free of unwrapping errors in the clinically relevant brain regions, and which provided a plausible basis for distortion correction of the fMRI data in all cases. The accuracy of the DDC was carefully assessed for each patient and compared to SDC results.

Fig. 2 illustrates SDC and DDC VSMs alongside the distortion-free reference (GE), and the temporal averages of the EPI with no application of distortion correction (noDC), and the static (SDC) and dynamically distortion-corrected (DDC) EPI for each patient. The VSMs from the DDC method were averaged over the time series of all runs and the corresponding temporal standard deviation was also calculated. In Fig. 2, a slice is shown in which the most statistically significant motor activation was detected for each patient (with the primary motor hand area delimited by green horizontal lines).

Overall, correcting for susceptibility-related distortion resulted in shifts towards the posterior (negative values in the VSMs) in the primary motor hand area. Large average shifts, of circa 4 mm (~2 voxels), were observed in three patients (P3, P4, and P7). In P3, a large region of susceptibility-related distortion is visible in the mean uncorrected EPI (at white arrow), where voxel shift values reached 5 mm (~3 voxels). These were corrected accurately by DDC (c.f. mean EPI (DDC) and GE), whereas with SDC some residual distortion is still visible (c.f. mean EPI (SDC) and GE). Smaller shifts, of circa 2 mm (~1-1.5 voxels), were present in four patients (P2, P5, P6, and P10) and negligible shifts (i.e. ~0–0.5 voxels) were observed in the remaining four patients (P1, P8, P9, and P11). The standard deviation of VSM values over time (std VSM) was circa 0.5 mm in the motor area in three patients (P1, P3, and P9) and close to 0 in the remaining patients (P2, P4-P8, P10, and P11). Relatively

larger std VSM values of circa 0.5– 1.0 mm were observed in the vicinity of the pathology (P2, P3, P6, P8, and P11).

In summary, application of the VSMs to the EPI time series resulted in correct repositioning of the primary motor hand area (judged by the GE reference image) in all patients and is particularly apparent in those where the largest shifts occurred (see P3, P4, and P7 in Fig. 2).

3.2 Shifts in activation

The primary motor cortex (M1) is one of the key areas involved in motor function. This functional region is located in the frontal lobe, along the precentral gyrus immediately anterior to the central sulcus. Execution of a motor task elicits activation in this area. Generally, SDC and DDC of the EPI time series resulted in repositioning of functional activation to a more physiologically meaningful location with regards to the GE reference image, i.e. precisely overlaying the underlying motor cortex in the GE. These shifts in the anterior-posterior direction were observed both in the most significantly activated voxels as well as in the bulk activation (Figs. 3–5). Anterior-posterior profiles of t-values through the most statistically significant motor activation reveal shifts of approximately 2 voxels (3.4 mm) in patients P4 (Fig. 5), P7 and P10 (Fig. 4), reaching over 3 voxels (5.1 mm) in more lateral areas of the primary motor cortex in P3 (Fig. 5). Shifts were smaller, namely ~1 voxel (1.7 mm), in P1, P5, P6 (Fig. 3), and P11 (Fig. 4), and negligible in P8 (Fig. 4). In P2 (Fig. 3), SDC led to a larger (~2 voxels) shift in activation than DDC. Nevertheless, unambiguous identification of the central sulcus was attainable in both cases. Particularly in P3 (Fig. 5), activation was mislocalized into a region of very strong signal loss without distortion correction. Following DDC, activation was repositioned to perfectly overlay M1. In the SDC case, the correction performed to a lesser extent, with activation partially overlaying the susceptibility artifact region (c.f. unthresholded SDC activation map and GE). In all cases, DDC did not lead to an apparent change in the width of the activation profiles. A modest enlargement in the activation profile was observed, however, in P6 with SDC.

3.2.1 Potential clinical implications of shifts in activation—

In presurgical planning, the aim is to precisely localize a functional region and preserve it during the operation to minimize the risk of post-surgical deficits. The mislocalization of functional activation observed may have clinical implications in this context. This applies particularly to the larger shifts in activation, of approximately 3.4 to 5.1 mm, for P3 and P4 (Section 3.2) (both shown in Fig. 5).

In patient P3, the peak activation in the thresholded noDC map is located in an area affected by strong susceptibility-related artifacts (Fig. 5, left column). Lowering the threshold shows this activation cluster to extend along the edge of the brain (Fig. 5, middle column). As such, it may wrongly be judged to originate from the susceptibility artefact (e.g. as a stimulus-correlated motion effect (Hajnal et al., 1994)). With distortion correction, however, that peak activation is relocated to perfectly overlay the primary motor cortex with DDC, and apart for some residual distortion, with SDC. At lower thresholds, the activation clearly follows the shape of the “inverted omega” (primary representation of the hand), indicating that this activation is genuine primary motor cortex activity.

In patient P4, with noDC, the most statistically significant activation appeared to be in the middle (most dorsal) part of the precentral gyrus, making the identification of the central sulcus problematic. The activation could be interpreted as reflecting viable primary motor cortex. Following distortion correction, resulting activation was shifted into the post-central gyrus, a correction which has been established as being accurate (Section 3.1, Fig. 2). In this case, distortion correction is likely to change the clinician's interpretation to suggest that, in fact, primary motor cortex is compromised, and function has been subsumed by the post-central gyrus (somatosensory motor cortex).

4 Discussion and Conclusion

In this study, the extent of distortion in EPI at UHF has been assessed and the potential clinical implications of disregarding correction for these distortions investigated in the context of simulated presurgical fMRI at UHF (7 T). A previous study by Beisteiner et al. (2011) has compared the functional sensitivity at UHF (7 T) against lower field strength (3 T). Benefits such as increased percent signal change, magnitude and extent of the activation, and contrast to noise ratio were reported. In that study, 7 T results suffered from increased artifact contamination (Nyquist ghosting and motion). Improvement to the Nyquist ghost correction approach have been made subsequently via implementation of a local phase correction (Feiweier, 2011). Beisteiner et al. (2011) did not assess the magnitude of distortions in EPI originated by increased B_0 inhomogeneity at 7 T and their clinical consequences. That issue was addressed in this study.

A state-of-the-art dynamic distortion correction method based on unmodified single-echo EPI was chosen as primary means for correcting distortions in clinical fMRI data. Results were compared with a conventional static distortion correction approach. It was possible to generate time series of EPI-based field maps which were artifact-free in eloquent brain areas from the fMRI phase data for all patients, despite the presence of signal dropouts caused by pathologies and post-operative sites, which pose a significant unwrapping challenge. Measurable distortions up to 5.1 mm were observed in the primary motor cortex. These were accurately corrected with the DDC and, to a lesser extent, with the SDC. The dynamic nature of distortion in the vicinity of pathologies and in the presence of unintentional motion in UHF clinical fMRI was reflected in the higher values in the standard deviation of the VSMs. In some patients, the correction was potentially clinically significant in that it might affect the localization or interpretation of activation and could thereby influence the treatment plan.

Deviations from B_0 of up to 65 Hz were observed around the central sulcus, even in the primary motor cortex, which is generally considered to be well shimmable. These led to sizeable distortions (varying from 1 to 3 voxels; 1.7–5.1 mm) despite the use of parallel imaging. Distortion was, however, corrected accurately with the DDC and fairly accurately with the SDC, as was demonstrated by the good correspondence to a near distortion-free GE reference image. Shifts in both EPI geometry and functional results are consistent with findings from previous studies in healthy volunteers (Dymerska et al., 2016b; Visser et al., 2012) and in patients investigated at 7 T (Dymerska et al., 2014; Robinson et al., 2010). Larger distortions have also been observed in other cortical regions (e.g. in the frontal lobe

close to the paranasal sinuses and ear canals). These were not explored further in this study as the focus was on the potential clinical implications of not correcting for susceptibility-related distortion in preoperative fMRI, but have been comprehensively documented in healthy volunteers by Dymerska et al. (2016a). Those findings indicate that the advantages of DDC over SDC are expected to be of equal or higher relevance in presurgical tasks which activate more ventral language and memory areas.

The relevance of correcting for susceptibility-related distortion has been investigated in prior simulated presurgical planning fMRI studies with neurological patients at 7 T, where distortions of circa 4 mm (Dymerska et al., 2014) or even larger (Robinson et al., 2010) were observed and corrected with SDC. In one case, a shift as large as ~1.8 mm away from the pathology suggested a more aggressive resection of the compromised tissue (Dymerska et al., 2014). In another, a shift of 5–7 mm may have indicated the necessity of a more conservative surgical approach or alternative treatment (Robinson et al., 2010). In either case, shifts of this extent could lead to a misidentification of the central sulcus – the relevant anatomical landmark for motor function. Tissue displacements greater than 10 mm have been reported due to brain surface deformation following craniotomy. Such shifts are to be considered separately from localization errors, however, as reference points identified correctly immediately after craniotomy may be tracked despite deformation during the surgical procedure (Hill et al., 1998; Roberts et al., 1998).

A dynamic approach to correcting for distortions was primarily used in this study because “static” approaches do not account for dynamic changes in B_0 originated by unintentional or task-related motion (Jezzard and Clare, 1999), hardware heating (Foerster et al., 2005) or respiration (Dymerska et al., 2016b; Zahneisen et al., 2014; Zeller et al., 2014). A study comparing SDC and a different DDC approach based on TE which is “jittered” between odd and even volumes has shown that in the presence of motion, SDC led to errors of up to 1.6 mm in the central sulcus even for head rotations as small as circa 0.8° (Dymerska et al., 2016b). Residual motion was also apparent in our study, even though motion of the head was minimized using plaster helmets. The average (over patients) of the maximum cumulative rotation was 2.48° ± 0.94°, with the absolute maximum cumulative motion 3.58° in P8. The DDC applied here has been shown to be robust to head rotations larger than those observed in this study, however. In two patients (P1 and P9), larger temporal standard deviation of the VSMs throughout the brain were observed. Continuous, low amplitude unintentional motion across the EPI volumes was observed in the same patients, exhibiting the high sensitivity of distortion to motion. In the presence of larger motion, SDC based on a single reference field map would not be likely to correct the resulting dynamic variations in the field distribution. An additional disadvantage of the SDC approach is the blurring of gray/white matter boundaries (Dymerska et al., 2016a), broadening of the activation, and unwarping errors (of ~1.6 mm) around the central sulcus (Dymerska et al., 2016b). This has not been observed with the DDC in this cohort of patients, although observed in one patient with the SDC, confirming this advantage over SDC.

To our knowledge, this is the first investigation of temporal B_0 variations in a patient population as well as at UHF (7 T). In five patients, the temporal standard deviations in the VSMs were larger in the vicinity of pathologies, indicating discernable field fluctuations in

these regions across the fMRI acquisition. Depending on their extent, the SDC may fail to correct these.

In this implementation of the DDC, a large amount of phase and magnitude data – that from all RF coils, without combination – needs to be exported from the image reconstructor and processed offline. The generation of time series of field maps is also time-consuming due to the need to generate masks and unwrap EPI phase images for each time point. In theory, this could lead to a less robust outcome for DDC than for SDC – despite the advantages of the DDC – because the EPI-based images used in DDC have lower SNR than the GE-based images used for the static correction, making them more prone to unwrapping errors. In this study, however, the unwrapping procedure proved robust, despite pathologies, and reliable field maps could be calculated for all patients. Further development and adaptation of the method, with on-scanner generation of offset-free phase images (or field maps), would be advantageous, and would aid adoption in clinical contexts.

Rigid body registration was used in this study to align EPI and reference scans. Affine transformation is typically used for this purpose but was not applied here as it introduces image stretches and shears which would make it impossible to isolate B_0-related distortion and the effectiveness of distortion correction. Affine transformation is also not able to correct the complex distortions encountered in EPI, particularly in clinical cases. Non-linear registration such as FNIRT (Jenkinson et al., 2002) or other methods (Bhushan et al., 2015; Chambers et al., 2015) could potentially remove complex distortions but these were not used here, as these are approaches which are non-standard and poorly tested, particularly in pathological brains.

The licensing of 7 T for diagnostic use is anticipated in the foreseeable future. Until then, such systems remain “research-only”. This study was conducted in line with current clinical practice for presurgical planning in our hospital (including protocols, paradigms, and analysis), but was nonetheless a simulation of presurgical planning, in that the results did not influence patient management in any way. Nevertheless, this constitutes a realistic representation of the distortions encountered in patient populations and the efficacy of distortion correction at ultra-high field.

In general, presurgical fMRI relies strongly on the experience and expertise of the assessing clinician and the availability of other imaging and diagnostic information (Stippich et al., 2015). Moreover, pathological conditions may induce variation in the localization and extent of activated regions, and mass effects and lesion-induced hemodynamic alterations may give rise to neuroplastic changes (Fraga de Abreu et al., 2016; Holodny et al., 1999; Holodny et al., 2000). Therefore, presurgical fMRI benefits from analysis using hemodynamic response functions with different timings or shapes at various thresholds (Beisteiner et al., 2000), and/or evaluated with model-free methods such as Independent Component Analysis (Robinson et al., 2013) and UNBIASED (Cardoso et al., 2016). Intraoperative electrocortical stimulation (ECS) is the ‘gold standard’ and most accurate procedure for identifying functionally relevant brain structures in a surgical context (i.e. those that if damaged would result in a substantial reduction in the quality of life of the patient). A limitation of this study

Europe PMC Funders Author Manuscripts

is that no ECS information is available for these patients due to the simulated nature of the study.

We have investigated the effectiveness and clinical relevance of correcting fMRI data for susceptibility-related distortions in a group of patients with a range of neuropathologies examined at 7 T while performing a motor task. To our knowledge, this is the first full report of the potential clinical relevance of distortion correction in UHF preoperative fMRI and the first to assess DDC in a clinical cohort. If no distortion correction was applied, shifts in activation in the primary motor region were observed which could affect decisions about the optimal therapeutic approach and treatment plan. The DDC is shown to effectively restore the anatomical representation and activation to the undistorted location.

Acknowledgements

This study was funded by the Austrian Science Fund (FWF) project KLI264. BD was additionally supported by a DOC fellowship of the Austrian Academy of Sciences. We are grateful to Prof. Dr. Christine Marosi for helping with the selection and recruitment of the patients who participated in this study.

References

Adcock JE, Wise RG, Oxbury JM, Oxbury SM, Matthews PM. Quantitative fMRI assessment of the differences in lateralization of language-related brain activation in patients with temporal lobe epilepsy. NeuroImage. 2003; 18:423–438. [PubMed: 12595196]

Andersson JL, Hutton C, Ashburner J, Turner R, Friston K. Modeling geometric deformations in EPI time series. NeuroImage. 2001; 13:903–919. [PubMed: 11304086]

Beisteiner R, Lanzenberger R, Novak K, Edward V, Windischberger C, Erdler M, Cunnington R, Gartus A, Streibl B, Moser E, Czech T, et al. Improvement of presurgical patient evaluation by generation of functional magnetic resonance risk maps. Neurosci Lett. 2000; 290:13–16. [PubMed: 10925163]

Beisteiner R, Robinson S, Wurnig M, Hilbert M, Merksa K, Rath J, Hollinger I, Klinger N, Marosi C, Trattnig S, Geissler A. Clinical fMRI: evidence for a 7T benefit over 3T. NeuroImage. 2011; 57:1015–1021. [PubMed: 21620980]

Bhushan C, Haldar JP, Choi S, Joshi AA, Shattuck DW, Leahy RM. Co-registration and distortion correction of diffusion and anatomical images based on inverse contrast normalization. NeuroImage. 2015; 115:269–280. [PubMed: 25827811]

Binder JR, Swanson SJ, Hammeke TA, Morris GL, Mueller WM, Fischer M, Benbadis S, Frost JA, Rao SM, Haughton VM. Determination of language dominance using functional MRI: a comparison with the Wada test. Neurology. 1996; 46:978–984. [PubMed: 8780076]

Cardoso PL, Fischmeister FP, Dymerska B, Geissler A, Wurnig M, Trattnig S, Beisteiner R, Robinson SD. Improving the clinical potential of ultra-high field fMRI using a model-free analysis method based on response consistency. Magn Reson Mater Phys. 2016; 29:435–449.

Chambers, MC., Bhushan, C., Haldar, JP., Leahy, RM., Shattuck, DW. Correcting inhomogeneity-induced distortion in FMRI using non-rigid registration. Proceedings of the 12th International Symposium on Biomedical Imaging (ISBI). IEEE; 2015. p. 1364-1367.

Cusack R, Brett M, Osswald K. An evaluation of the use of magnetic field maps to undistort echo-planar images. NeuroImage. 2003; 18:127–142. [PubMed: 12507450]

De Panfilis C, Schwarzbauer C. Positive or negative blips? The effect of phase encoding scheme on susceptibility-induced signal losses in EPI. NeuroImage. 2005; 25:112–121. [PubMed: 15734348]

Dymerska, B., Fischmeister, F., Geissler, A., Matt, E., Trattnig, S., Beisteiner, R., Robinson, SD. Clinical relevance of EPI distortion correction in presurgical fMRI at 7 T. Proceedings of the 22nd Annual Meeting of the ISMRM. 2014. p. 1416

Dymerska B, Poser BA, Barth M, Trattnig S, Robinson SD. A method for the dynamic correction of B0-related distortions in single-echo EPI at 7T. NeuroImage. 2016a; doi: 10.1016/j.neuroimage.2016.07.009

Dymerska B, Poser BA, Bogner W, Visser E, Eckstein K, Cardoso P, Barth M, Trattnig S, Robinson SD. Correcting dynamic distortions in 7T echo planar imaging using a jittered echo time sequence. Magn Reson Med. 2016b; 76:1388–1399. [PubMed: 26584148]

Edward V, Windischberger C, Cunnington R, Erdler M, Lanzenberger R, Mayer D, Endl W, Beisteiner R. Quantification of fMRI artifact reduction by a novel plaster cast head holder. Hum Brain Mapp. 2000; 11:207–213. [PubMed: 11098798]

Feiweier T. Magnetic resonance method and apparatus to determine phase correction parameters. 2011 Google Patents.

Foerster BU, Tomasi D, Caparelli EC. Magnetic field shift due to mechanical vibration in functional magnetic resonance imaging. Magn Reson Med. 2005; 54:1261–1267. [PubMed: 16215962]

Fraga de Abreu VH, Peck KK, Petrovich-Brennan NM, Woo KM, Holodny AI. Brain tumors: the influence of tumor type and routine MR imaging characteristics at BOLD functional MR imaging in the primary motor gyrus. Radiology. 2016; 281:876–883. [PubMed: 27383533]

Garcia D. Robust smoothing of gridded data in one and higher dimensions with missing values. Comput Stat Data Anal. 2010; 54:1167–1178. [PubMed: 24795488]

Hahn AD, Nencka AS, Rowe DB. Improving robustness and reliability of phase-sensitive fMRI analysis using temporal off-resonance alignment of single-echo timeseries (TOAST). NeuroImage. 2009; 44:742–752. [PubMed: 18992826]

Hajnal J, Myers R, Oatridge A, Schwieso J, Young I, Bydder G. Artifacts due to stimulus correlated motion in functional imaging of the brain. Magn Reson Med. 1994; 31:283–291. [PubMed: 8057799]

Hill DL, Maurer CR Jr, Maciunas RJ, Barwise JA, Fitzpatrick JM, Wang MY. Measurement of intraoperative brain surface deformation under a craniotomy. Neurosurgery. 1998; 43:514–526. [PubMed: 9733307]

Holodny AI, Schulder M, Liu WC, Maldjian JA, Kalnin AJ. Decreased BOLD functional MR activation of the motor and sensory cortices adjacent to a glioblastoma multiforme: implications for image-guided neurosurgery. AJNR Am J Neuroradiol. 1999; 20:609–612. [PubMed: 10319970]

Holodny AI, Schulder M, Liu WC, Wolko J, Maldjian JA, Kalnin AJ. The effect of brain tumors on BOLD functional MR imaging activation in the adjacent motor cortex: implications for image-guided neurosurgery. AJNR Am J Neuroradiol. 2000; 21:1415–1422. [PubMed: 11003273]

Hutton C, Bork A, Josephs O, Deichmann R, Ashburner J, Turner R. Image distortion correction in fMRI: a quantitative evaluation. NeuroImage. 2002; 16:217–240. [PubMed: 11969330]

Jenkinson M. Fast, automated, N-dimensional phase-unwrapping algorithm. Magn Reson Med. 2003; 49:193–197. [PubMed: 12509838]

Jenkinson M, Bannister P, Brady M, Smith S. Improved optimization for the robust and accurate linear registration and motion correction of brain images. NeuroImage. 2002; 17:825–841. [PubMed: 12377157]

Jezzard P, Balaban RS. Correction for geometric distortion in echo planar images from B0 field variations. Magn Reson Med. 1995; 34:65–73. [PubMed: 7674900]

Jezzard P, Clare S. Sources of Distortions in Functional MRI Data. Hum Brain Mapp. 1999; 8:80–85. [PubMed: 10524596]

Kashida Y, Otsubo T, Hanaya R, Kodabashi A, Tsumagari N, Sugata S, Hosoyama H, Iida K, Nakamura K, Tokimura H, Fujimoto T, et al. Determination of hemispheric language dominance using functional magnetic resonance imaging and the Shiritori (Japanese word chain) task in patients with epilepsy: comparison with the Wada test. Epilepsy Res. 2016; 124:16–22. [PubMed: 27185362]

Lamberton F, Delcroix N, Grenier D, Mazoyer B, Joliot M. A new EPI-based dynamic field mapping method: application to retrospective geometrical distortion corrections. J Magn Reson Imaging. 2007; 26:747–755. [PubMed: 17729370]

Lehericy S, Duffau H, Cornu P, Capelle L, Pidoux B, Carpentier A, Auliac S, Clemenceau S, Sichez JP, Bitar A, Valery CA, et al. Correspondence between functional magnetic resonance imaging somatotopy and individual brain anatomy of the central region: comparison with intraoperative stimulation in patients with brain tumors. J Neurosurg. 2000; 92:589–598. [PubMed: 10761647]

Marques, JP., Bowtell, R. Evaluation of a new method to correct the effects of motion-induced B0-field variation during fMRI. Proceedings of the 13th meeting of the ISMRM. 2005. p. 510

Ooi MB, Muraskin J, Zou X, Thomas WJ, Krueger S, Aksoy M, Bammer R, Brown TR. Combined prospective and retrospective correction to reduce motion-induced image misalignment and geometric distortions in EPI. Magn Reson Med. 2013; 69:803–811. [PubMed: 22499027]

Poser BA, Norris DG. Investigating the benefits of multi-echo EPI for fMRI at 7 T. NeuroImage. 2009; 45:1162–1172. [PubMed: 19349231]

Roberts DW, Hartov A, Kennedy FE, Miga MI, Paulsen KD. Intraoperative brain shift and deformation: a quantitative analysis of cortical displacement in 28 cases. Neurosurgery. 1998; 43:749–758. [PubMed: 9766300]

Robinson, S., Geissler, A., Trattnig, S., Beisteiner, R. Correcting for EPI distortion at very high field using the fieldmap method with multi-channel coils: effectiveness in presurgical planning fMRI at 7 T. Proceedings of the 18th Annual Meeting of the ISMRM. 2010. p. 2302

Robinson S, Grabner G, Witoszynskyj S, Trattnig S. Combining phase images from multi-channel RF coils using 3D phase offset maps derived from a dual-echo scan. Magn Reson Med. 2011; 65:1638–1648. [PubMed: 21254207]

Robinson S, Jovicich J. B0 mapping with multi-channel RF coils at high field. Magn Reson Med. 2011; 66:976–988. [PubMed: 21608027]

Robinson SD, Bredies K, Khabipova D, Dymerska B, Marques JP, Schweser F. An illustrated comparison of processing methods for MR phase imaging and QSM: combining array coil signals and phase unwrapping. NMR Biomed. 2016; doi: 10.1002/nbm.3601

Robinson, SD., Dymerska, B., Trattnig, S. Improving the accuracy of 2D phase unwrapping using a triplanar approach. Proceedings of the 22nd Annual Meeting of the ISMRM. 2014. p. 3262

Robinson SD, Schopf V, Cardoso P, Geissler A, Fischmeister FP, Wurnig M, Trattnig S, Beisteiner R. Applying independent component analysis to clinical FMRI at 7 T. Front Hum Neurosci. 2013; 7:496. [PubMed: 24032007]

Scharnhorst K. Angles in complex vector spaces. Acta Appl Math. 2001; 69:95–103.

Stevens MT, Clarke DB, Stroink G, Beyea SD, D'Arcy RC. Improving fMRI reliability in presurgical mapping for brain tumours. J Neurol Neurosurg Psychiatry. 2016; 87:267–274. [PubMed: 25814491]

Stippich, C., Blatow, M., Garcia, M. Task-based presurgical functional MRI in patients with brain tumors. Clinical Functional MRI. Stippich, C., editor. Springer; Berlin, Heidelberg: 2015. p. 89-141.

Triantafyllou C, Hoge RD, Krueger G, Wiggins CJ, Potthast A, Wiggins GC, Wald LL. Comparison of physiological noise at 1.5 T, 3 T and 7 T and optimization of fMRI acquisition parameters. NeuroImage. 2005; 26:243–250. [PubMed: 15862224]

van der Zwaag W, Francis S, Head K, Peters A, Gowland P, Morris P, Bowtell R. fMRI at 1.5, 3 and 7 T: characterising BOLD signal changes. NeuroImage. 2009; 47:1425–1434. [PubMed: 19446641]

Visser E, Poser BA, Barth M, Zwiers MP. Reference-free unwarping of EPI data using dynamic off-resonance correction with multiecho acquisition (DOCMA). Magn Reson Med. 2012; 68:1247–1254. [PubMed: 22851507]

Weiskopf N, Klose U, Birbaumer N, Mathiak K. Single-shot compensation of image distortions and BOLD contrast optimization using multi-echo EPI for real-time fMRI. NeuroImage. 2005; 24:1068–1079. [PubMed: 15670684]

Zahneisen B, Asslander J, LeVan P, Hugger T, Reisert M, Ernst T, Hennig J. Quantification and correction of respiration induced dynamic field map changes in fMRI using 3D single shot techniques. Magn Reson Med. 2014; 71:1093–1102. [PubMed: 23716298]

Zeller M, Kraus P, Muller A, Bley TA, Kostler H. Respiration impacts phase difference-based field maps in echo planar imaging. Magn Reson Med. 2014; 72:446–451. [PubMed: 24018714]

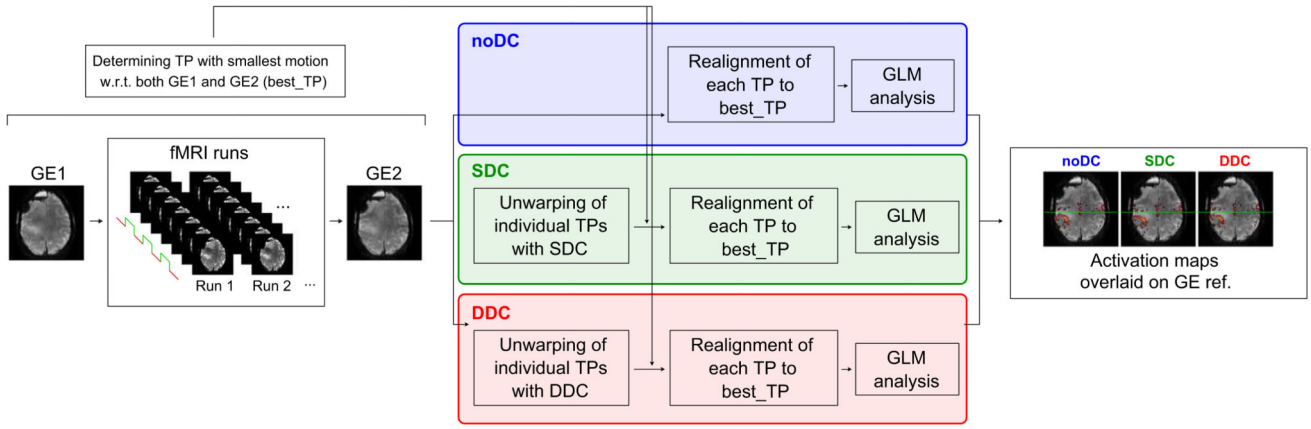

Fig. 1.

Schematic overview of the steps applied in the analysis of patient data, from acquisition to final activation maps. Analysis for no distortion correction (noDC) (*blue*), static (SDC) (*green*), and dynamic distortion correction (DDC) (*red*) differs only in the unwarping of individual time points (TPs) in the SDC and DDC pipelines. In SDC, a GE-based field map is used for unwarping the EPI TPs; in DDC, an EPI-based field map per TP is used.

Europe PMC Funders Author Manuscripts

Europe PMC Funders Author Manuscripts

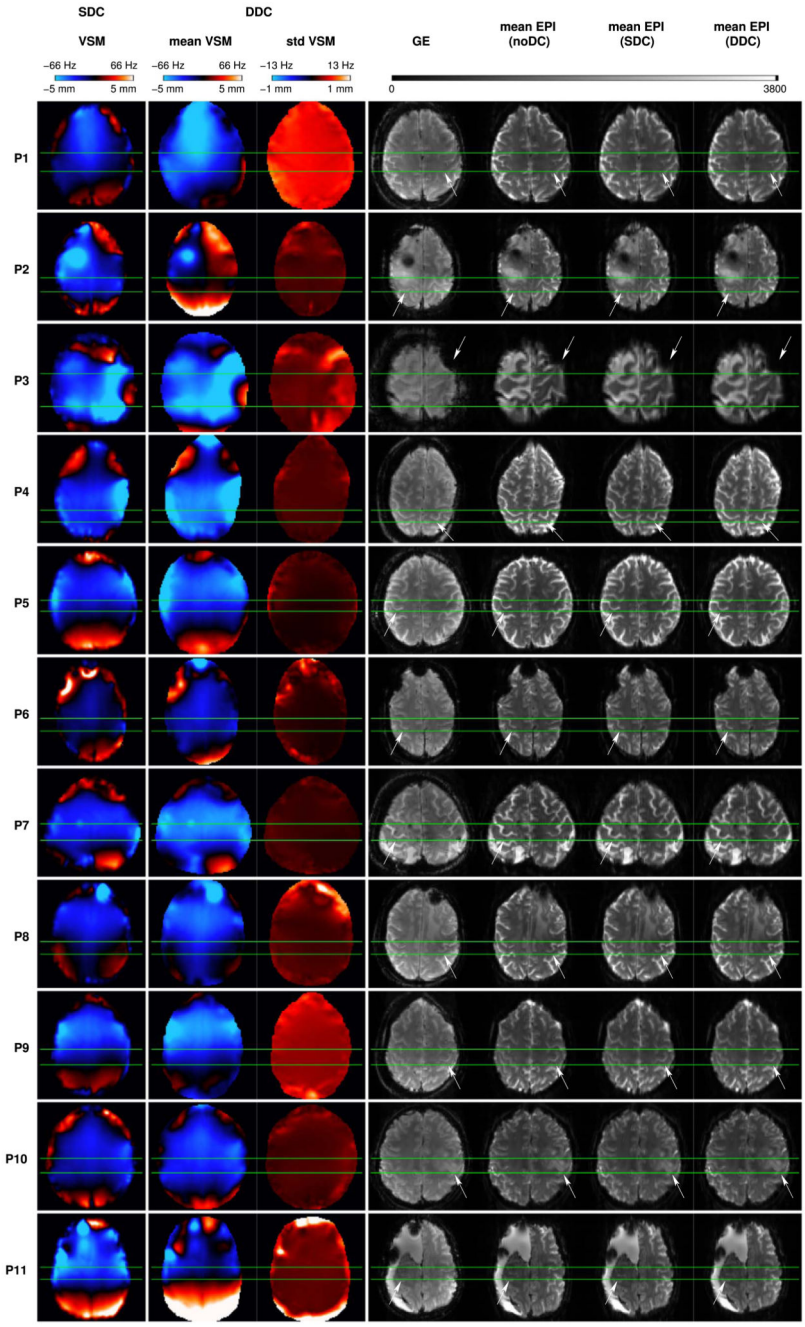

Fig. 2.

Left column: SDC VSMs for all patients in a slice in which the most statistically significant motor activation was detected. *Middle column*: Temporal mean (*left*) and standard deviation (*right*) over the time series for all runs of the DDC VSMs in the same slice. Color bars indicate both values of ΔB_0 in Hz and shifts in mm for the echo spacing used in this study. *Right column*: GE distortion-free reference, and mean temporal images for noDC, SDC, and DDC EPI in the same slice. *Green lines* delimit the primary motor hand area of the affected side (at *white arrows*). Radiological convention is used.

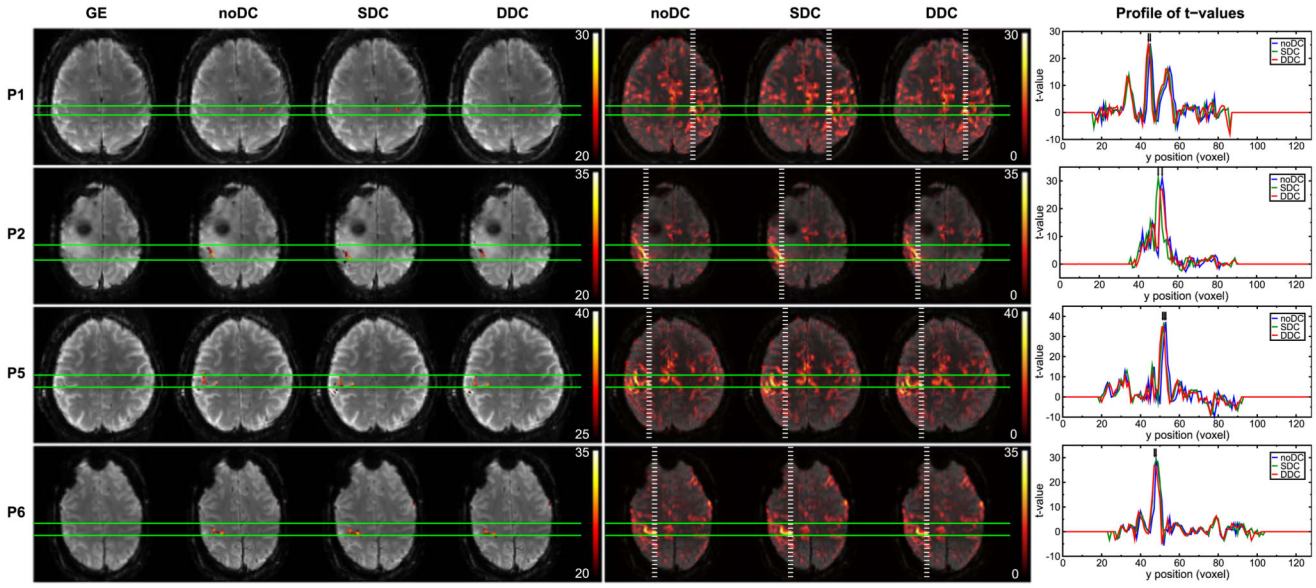

Fig. 3.

Comparison of noDC, SDC, and DDC for 4 patients. Patients P3 and P4 are illustrated in a dedicated figure (Fig. 5). Potentially clinical relevant shifts were found in these two cases and are described in Section 3.2.1. *Left column*: GE reference and thresholded activation maps obtained from noDC, SDC, and DDC analyses. *Middle column*: Unthresholded positive t-values for noDC, SDC, and DDC. Images are presented with a transparency of 25%. *Right column*: Plots of the t-values for noDC (*blue*), SDC (*green*), and DDC (*red*) along the dashed white lines (in posterior-anterior direction) on the full range maps of activation (*middle column*). Images are presented in radiological convention.

Europe PMC Funders Author Manuscripts

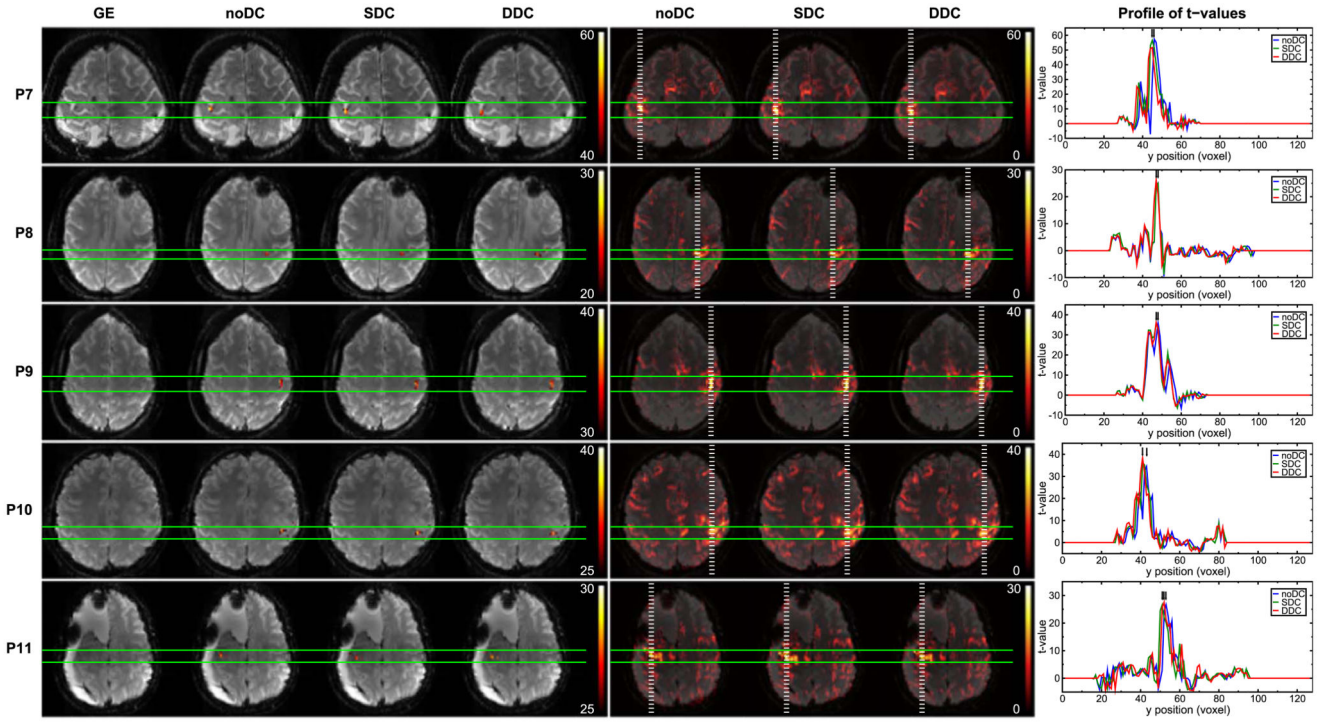

Fig. 4.

Comparison of noDC and DDC for 5 patients. *Left column*: GE reference and thresholded activation maps obtained from noDC, SDC, and DDC analyses. *Middle column*: Unthresholded positive t-values for noDC, SDC, and DDC. Images are presented with a transparency of 25%. *Right column*: Plots of the t-values for noDC (*blue*), SDC (*green*), and DDC (*red*) along the dashed white lines (in posterior-anterior direction) on the full range maps of activation (*middle column*). Images are presented in radiological convention.

Europe PMC Funders Author Manuscripts

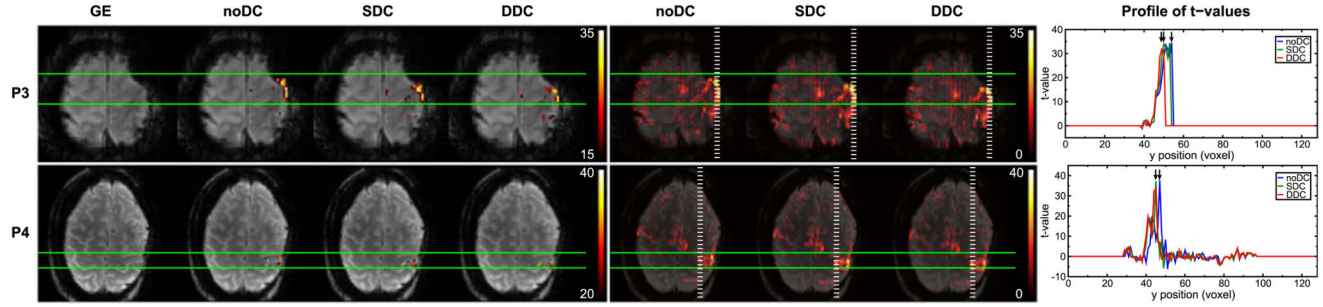

Fig. 5.

Comparison of noDC, SDC, and DDC for 2 patients with potential clinically relevant shifts in activation. *Left column*: GE reference and thresholded activation maps obtained from noDC, SDC, and DDC analyses. *Middle column*: Unthresholded positive t-values for noDC, SDC, and DDC. Images are presented with a transparency of 25%. *Right column*: Plots of the t-values for noDC (*blue*), SDC (*green*), and DDC (*red*) along the dashed white lines (in posterior-anterior direction) on the full range maps of activation (*middle column*). Images are presented in radiological convention.

Europe PMC Funders Author Manuscripts

Europe PMC Funders Author Manuscripts

Table 1

Patient demographics and clinical information. Patient IDs were attributed in chronological data acquisition order and are used in subsequent images and descriptions in the text.

Patient ID	Age	Gender	Affected hand	Pathology
P1	58	F	R	Developmental venous anomaly, left insular cortex
P2	34	M	L	2 oligodendrogliomas grade II, 1 right frontal, 1 right central
P3	55	F	R	Secondary glioblastoma, left temporal
P4	37	F	R	Glioblastoma, left temporo-frontal
P5	52	F	L	Anaplastic astrocytoma grade III, right temporo-occipital
P6	30	M	L	Anaplastic astrocytoma, right frontal
P7	55	M	L	Oligoastrocytoma, right occipital, with multiple bilateral metastases
P8	58	F	R	Anaplastic oligodendroglioma grade III, left frontal
P9	33	F	R	Arteriovenous malformation, left hemisphere
P10	46	M	R	Suspected low grade glioma, precentral left
P11	34	M	L	Oligoastrocytoma, right frontal